ARCHIVES OF ELECTRICAL ENGINEERING VOL. 72(1), pp. 103–124 (2023)

DOI 10.24425/aee.2023.143692

Online control signal-based diagnosis of interturn short circuits of PMSM drive

MATEUSZ KRZYSZTOFIAK, TOMASZ ZAWILAK, GRZEGORZ TARCHAŁA ✉

Wrocław University of Science and Technology
Department of Electrical Machines, Drives and Measurements
Wybrzeże Wyspiańskiego 27, 50-370 Wrocław, Poland
e-mail: grzegorz.tarchala@pwr.edu.pl

(Received: 07.08.2022, revised: 20.10.2022)

Abstract: Modern drives with Permanent Magnet Synchronous Motors (PMSMs) require both efficient control structure to ensure excellent dynamics and effective diagnostic algorithms to detect the motor faults that can occur. This paper shows the combination of both mentioned aspects – the direct-axis based signals of the Field Oriented Control (FOC) structure are proposed as diagnostic signals to allow diagnosing the interturn short-circuit failure that can appear inside stator windings. The amplitudes of second order harmonics are selected as the fault indicators. Different modelling methods are analysed and compared in detail in this paper: an analytical mathematical model, a Finite Element Method (FEM)-based model and next verified using a laboratory setup. The results obtained using all the mentioned models proved that the proposed fault indices are increasing significantly with the number of shorted turns and are independent on the load torque level.

Key words: decoupling, diagnostic, FEM, interturn short circuits, modelling, PMSM

Nomenclature

B	friction factor [Nm·s/rad]	R_{sA}, R_{sB}, R_{sC}	stator phase winding resistances [Ω]
E_{sd}, E_{sq}	decoupling signals [V]	T_e, T_l	electromagnetic and load torques [Nm]
$\boldsymbol{E_{sf}}$	back-EMF vector [V]	U_{sA}, U_{sB}, U_{sC}	phase voltages [V]
f_s	supply voltage frequency [Hz]	$\boldsymbol{U_{sf}}$	voltage vector [V]

© 2023. The Author(s). This is an open-access article distributed under the terms of the Creative Commons Attribution-NonCommercial-NoDerivatives License (CC BY-NC-ND 4.0, https://creativecommons.org/licenses/by-nc-nd/4.0/), which permits use, distribution, and reproduction in any medium, provided that the Article is properly cited, the use is non-commercial, and no modifications or adaptations are made.

www.czasopisma.pan.pl PAN POLSKA AKADEMIA NAUK www.journals.pan.pl

I_f	short-circuit current [A]	Ω_m, Ω_e	mechanical and electrical speed [rad/s]
$\boldsymbol{I_{sf}}$	stator current vector [A]	θ_m, θ_e	mechanical and electrical angle [rad]
I_{sA}, I_{sB}, I_{sC}	phase currents [A]	μ	relative number of shorted winding turns [–]
J	moment of inertia [kg·m^2]	Ψ_{sA}, Ψ_{sB}, Ψ_{sC}	stator phase magnetic flux [Wb]
$\boldsymbol{L_{sf}}$	stator inductance matrix [H]	$\boldsymbol{\Psi_{PMf}}$	permanent magnet flux vector [Wb]
L_{sA}, L_{sB}, L_{sC}	phase self-inductance [H]	Ψ_{PM}	magnetic flux induced by rotor magnets [Wb]
M_{sAB}, M_{sBA}, M_{sBC}, M_{sCB}, M_{sAC}, M_{sCA}	mutual inductances between phases [H]	$\boldsymbol{\Psi_{sf}}$	stator flux vector [Wb]
N_{sh}	number of shorted turns [–]	d-q	reference frame rotating with electrical motor speed
N	number of all turns in phase winding [–]	α-β	stationary reference frame
p_p	number of pole pairs [–]	ref	reference value
R_f	resistance of shorted loop [Ω]	N	nominal value
$\boldsymbol{R_{sf}}$	stator resistance matrix [Ω]		

1. Introduction

Interest in permanent magnet synchronous motors (PMSMs) is growing due to their many advantages: simple design, a small moment of inertia, high acceleration, high torque overload capacity, high power-to-weight ratio, wide speed range and high efficiency [1]. All of these advantages lead to the increasing use of the PMSM in electric cars, locomotives, aviation, or industrial production lines. The application of motors in such a multitude of applications and continuous operation, as well as environmental external factors, leads to many types of failure. Depending on the type of damage defects that occur in PMSMs, they are classified into electrical, mechanical, and magnetic faults [2]. Uncontrolled spread of failure can lead to complete destruction of the machine. For this reason, the diagnosis of electric drives is an important issue and one that is constantly being developed. In the literature, three main directions of diagnostics can be observed: diagnostics based on signal processing methods (the idea of which is to detect changes occurring in the signals available for measurement), artificial intelligence methods (the idea of which is to automatically detect damage without the human factor) and mathematical modelling (the idea of which is to create a mathematical version of the physical electric motor) [3].

According to the statistics presented in [4], the interturn short-circuit (ITSC) fault in electric motors occurs in 37% of medium-power motor faults, while they account for 66% of faults in high-voltage motors. The detection of winding short circuits is an important issue because the winding damage in a short time leads to destruction of the whole machine.

www.czasopisma.pan.pl PAN POLSKA AKADEMIA NAUK www.journals.pan.pl

In signal-based diagnostics, the analysis is based on the extraction of characteristic symptoms fault. The symptoms that accompany a failure can be obtained directly from a physically damaged motor. The other solution is to create mathematical models of the faulty motor. The examples of using the mathematical model are mostly focused on circuit models [5–16] and field-circuit models [17, 19–23]. Circuit models based on the equivalent motor circuit based on Kirchhoff's equations are most often presented in the ABC phase system [5–9]. Moreover, the analysis of the literature allows one to observe that the damage model of the PMSM can be presented also in the stationary reference frame α-β [8, 9] and synchronous rotating frame d-q [7–13]. Regardless of the reference frame, the presented models differ slightly from each other, the variations are mainly due to the mathematical notation. On the other hand, the second approach to simulate failures is to use field-circuit models. They are used in the design of new machines and can also be used for the analysis of interturn short-circuit failure. The model in this case consists of a field part and a circuit part. In the field part, a geometric representation of the motor model is created, onto which a computational mesh is superimposed. The electromagnetic field is then calculated at each resulting node. The circuit part contains a defined number of machine windings, the motor winding parameters, and the equation of motion that completes the entire dynamics of the object. The field-circuit calculation reflects the behaviour of the actual machine to a much more accurate degree.

Signal based methods use various signal processing methods, i.e. Fast Fourier Transform (FFT) [17, 20, 22] Short-Time Fourier Transform (STFT) [24], Wavelet Transform (WT) [24], the bispectrum method [25] or Extended Park Vector Approach (EPVA) [15]. The listed methods lead to the processing of the signal to be analysed and the subsequent extraction of motor fault symptoms. Based on the collected information, the technical condition of the machine can be deduced by observing the trend of individual symptoms changes. Artificial intelligence is also often used for inference. Classical neural networks [20], machine learning [26] and neural networks based on deep learning [17, 19] are currently used in the diagnostics.

The diagnostic systems are focusing on detecting failure at the earliest possible stage that leads to careful analysis and a fuzzy boundary between the diagnostic methods. More and more often combining the mathematical model and signal processing methods appears in the literature. The authors of [12] proposed the use of an analytical model to prepare a method for short-circuit fault detection based on the WT, but the order of the obtained results from the transform indicates an inaccuracy between the analytical model and the experimental motor. The use of the analytical model of the motor and a verification with usage of an experimental model of the motor is presented in [15]. The application of the EPVA method to diagnose inter-winding short circuits in a PMSM is also presented. It has been noted that the amplitude of the $2f_s$ harmonic component of the stator current EPVA signature is a useful indicator of the fault severity. Similarly, the authors of [9] use the double Park transformation of the voltage signal from the control system to formulate a diagnostic indicator to detect a PMSM winding short-circuit fault. Using signals from the control structure, the authors of [27] determined the active and reactive power consumed by the PMSM motor during different operating states based on the current and voltage vector in the d-q reference system. Also, the use of signals from the control structure to diagnose other (high resistance connection, misalignment, damaged bearing) faults in the PMSM is presented in [14] and [28–30].

www.czasopisma.pan.pl PAN POLSKA AKADEMIA NAUK www.journals.pan.pl

Industrial inverter-powered PMSMs in most cases have a direct field-oriented control (DFOC) structure implemented as default. Considerations for the control system and the search for symptoms in the control structure are presented in [10]. The authors of the paper constructed an indicator based on the signals from the control structure. The fault indicator is constructed from the product of the quotient of the second-order harmonic amplitudes of the voltage and current vector components in the d-q axes. The value of the indicator is shown to be constant over a wide range of bandwidths. However, analysis of the control system decoupling signals was left out.

This paper focuses on the comparison of an analytical, field-circuit model and an experimental PMSM motor for the search for symptoms of the ITSC. The possibility of detecting the stator winding faults based exclusively on signals from a closed field-oriented control structure, with and without decoupling of the rotor flux and torque control paths, is analysed. The proposed approach presents the use of fault symptoms and their visibility in mathematical models for subsequent use in PMSM motor diagnostics.

The article is divided into 7 parts. Section 2 presents an analytical and a field-circuit models. Section 3 presents the experimental stand as a starting point for comparing the presented models. Section 4 describes shortly the DFOC structure. Section 5 shows the ideas behind the machine condition assessment. Section 6, on the other hand, evaluates the degree of the damages and validates the described mathematical models for use in fault detection. Finally, Section 7 presents conclusions.

2. Modelling of PMSM stator winding short-circuit faults

During the operation, the drive can be exposed to tough operating conditions i.e. varying load, mechanical vibrations, high temperature or harsh work environment. The influence of these phenomena on the running motor leads to a gradual degradation of the motor insulation. Damage to the insulation of the winding causes an interturn short-circuit loop that can spread over the whole winding rapidly.

The mathematical model of a PMSM that allows one to model the interturn short-circuit damage is still being developed and expanded. The interest in modelling electrical faults is related to the possibility of simulating the physical motor without damaging it and performing tests in repeatable simulation conditions. There are two main approaches to create the damage models: analytical, circuit models [5–16] and FEM-circuit models, based on the Finite Element Method (FEM) combined with circuit models [17–23]. The selection of the model for the research depends mainly on the expectations of the researcher, such as computing power, the accuracy of reflecting phenomena occurring in the physical motor or a simulation time.

2.1. Analytical model of a faulty PMSM

The analytical model of a surface-mounted PMSM with interturn short-circuit fault requires adopting several simplifying assumptions, such as: no magnetic saturation, lumped windings with constant parameters and sinusoidal back-EMF. The model presented in this section is derived in an ABC natural system and written using vectors (indicated with a bold font). It is based on a commonly applied solution [7] and slightly extended here, to allow modelling the fault in each

www.czasopisma.pan.pl PAN POLSKA AKADEMIA NAUK www.journals.pan.pl

of the motor phase. In this case only the fundamental harmonic frequency is taken into account. The damage factor defined as $\mu = N_{sh}/N$, i.e. the ratio of the number of shorted turns to all turns in the phase winding, is used to define the severity of the damage.

A diagram of a wye-connected PMSM is presented in Fig. 1(a), while Fig. 1(b) shows the simplified diagram of a faulty phase, divided into an undamaged and a damaged part. The R_f resistance simulates faulty insulation. In this paper, it is assumed that during the fault $R_f \to 0$, which corresponds to a metallic connection. In this case voltage of the shorted circuit $U_f = 0$. Based on Fig. 1(a) and Fig. 1(b), using Kirchhoff's law, the following voltage equations can be written:

$$\boldsymbol{U_{sf}} = \boldsymbol{R_{sf}}\boldsymbol{I_{sf}} + \frac{\mathrm{d}\boldsymbol{\Psi_{sf}}}{\mathrm{d}t}, \tag{1}$$

where:

$$\boldsymbol{U_{sf}} = \begin{bmatrix} U_{sA} \\ U_{sB} \\ U_{sC} \\ U_f \end{bmatrix}, \quad \boldsymbol{R_{sf}} = \begin{bmatrix} R_{sA} & 0 & 0 & \mu_A R_{sA} \\ 0 & R_{sB} & 0 & \mu_B R_{sB} \\ 0 & 0 & R_{sC} & \mu_C R_{sC} \\ \mu_A R_{sA} & \mu_B R_{sB} & \mu_C R_{sC} & \mu_A R_{sX} + R_f \end{bmatrix},$$
$$\boldsymbol{I_{sf}} = \begin{bmatrix} I_{sA} \\ I_{sB} \\ I_{sC} \\ I_f \end{bmatrix}, \quad \boldsymbol{\Psi_{sf}} = \begin{bmatrix} \Psi_{sA} \\ \Psi_{sB} \\ \Psi_{sC} \\ \Psi_f \end{bmatrix}. \tag{2}$$

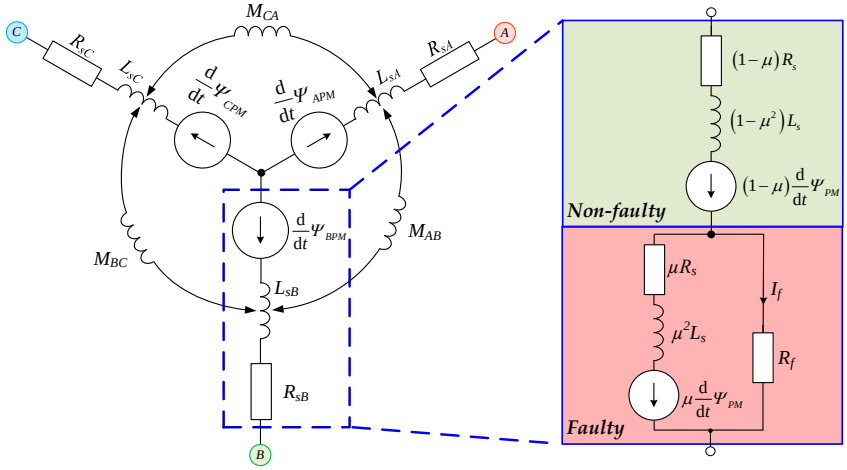

(a) (b)

Fig. 1. Diagram of a PMSM with interturn short-circuit fault: (a) wye-connected stator windings; (b) phase B divided into non-faulty and faulty parts

In the case of the fault occurring in phase A the parameter $\mu_A = \mu$, and $\mu_B = \mu_C = 0$. When the fault appears in phase B or C, $\mu_B = \mu$ and $\mu_C = \mu$, respectively. Symbol X indicates the faulty phase, i.e. $X = \{A, B, C\}$.

www.czasopisma.pan.pl PAN POLSKA AKADEMIA NAUK www.journals.pan.pl

The stator flux, when the fault occurs, consists in a part connected with stator current and the part related to the flux induced by permanent magnets:

$$\boldsymbol{\Psi}_{sf} = \boldsymbol{L}_{sf}\boldsymbol{I}_{sf} + \boldsymbol{\Psi}_{PMf}\,, \tag{3}$$

where:

$$\boldsymbol{L}_{sf} = \begin{bmatrix} L_{sA} & M_{sAB} & M_{sAC} & -\mu M_{sAX} \\ M_{sBA} & L_{sB} & M_{sBC} & -\mu M_{sBX} \\ M_{sCA} & M_{sCB} & L_{sC} & -\mu M_{sCX} \\ \mu M_{sXA} & \mu M_{sXB} & \mu M_{sXC} & -\mu^2 L_{sX} \end{bmatrix}, \qquad \boldsymbol{\Psi}_{PMf} = \begin{bmatrix} \Psi_{APM} \\ \Psi_{BPM} \\ \Psi_{CPM} \\ \Psi_{fPM} \end{bmatrix}. \tag{4}$$

When the fault takes place in phase A: $M_{sXA} = M_{sAA} = L_{sA}$, in phase B: $M_{sBB} = L_{sB}$ and C: $M_{sCC} = L_{sC}$. In the case of symmetrical motor windings: $R_s = R_{sA} = R_{sB} = R_{sC}$, $L_s = L_{sA} = L_{sB} = L_{sC}$ and $M_s = M_{sAB} = M_{sBA} = M_{sBC} = M_{sCB} = M_{sAC} = M_{sCA}$.

This assumption will be taken in the further part of the paper.

The magnetic flux linkage due to the presence of permanent magnets depends on the value of the rotor position related to the stator of the motor and is as follows:

$$\boldsymbol{\Psi}_{PMf} = \Psi_{PM}\left[\cos(\theta_e)\cos\left(\theta_e - \frac{2}{3}\pi\right)\cos\left(\theta_e - \frac{2}{3}\pi\right)\mu\cos(\theta_e + \theta_X)\right]^T, \tag{5}$$

where the electrical angle $\theta_e = p_p\theta_m$. The angle θ_X indicates the angle of the faulty phase, i.e. $\theta_X = \{\theta_A, \theta_B, \theta_C\} = \{0, -2/3\pi, 2/3\pi\}$, respectively.

Thus, taking into account the last row of (1), the following voltage equation of the short circuit (red part in Fig. 1(b)) can be derived:

$$\begin{aligned} U_f &= R_f I_f = \mu R_s\left(I_{sX} - I_f\right) - \mu^2 L_s\frac{\mathrm{d}I_f}{\mathrm{d}t} + \mu\boldsymbol{M}^T\frac{\mathrm{d}}{\mathrm{d}t}\boldsymbol{I}_s - \mu\omega_e\Psi_{PM}\sin(\theta_e + \theta_X)\,, \\ \boldsymbol{M} &= \begin{bmatrix} M_{sXA} & M_{sXB} & M_{sXC} \end{bmatrix}^T, \qquad \boldsymbol{I}_s = \begin{bmatrix} I_{sA} & I_{sB} & I_{sC} \end{bmatrix}^T. \end{aligned} \tag{6}$$

Electromagnetic torque is described by (7), while the induced back-emf voltage is expressed in (8):

$$T_e = \frac{\boldsymbol{E}_{sf}^T\boldsymbol{I}_{sf}}{\Omega_m}\,, \tag{7}$$

$$\boldsymbol{E}_{sf} = \frac{\mathrm{d}\boldsymbol{\Psi}_{PMf}}{\mathrm{d}t}\,. \tag{8}$$

The classical equation of motion complements the mathematical description of the faulty PMSM:

$$J\frac{\mathrm{d}}{\mathrm{d}t}\Omega_m = T_e - T_l - B\Omega_m\,, \tag{9}$$

$$\frac{\mathrm{d}\theta_m}{\mathrm{d}t} = \Omega_m\,. \tag{10}$$

2.2. Modelling based on FEM simulations

Under developing the field-circuit model of the PMSM, parameters of an industrial 2.5 kW Lenze MCS14H15 motor were used. These parameters are listed in Table 2 (Appendix). A cross-section visualization of the modelled motor is presented in Fig. 2. The stator has a concentrated type of winding, one phase comprises two coils, 125 turns each. Using the concentrated winding, the total harmonic distortion (THD) of air-gap flux density is greatly reduced compared to the distributed winding [23]. The rotor of the synchronous machine has magnets placed on the rotor surface. They are fixed with glue. In order to enable modelling of the damage as interturn short circuits, one, two and three turns were separated from one coil. During an undamaged operation, only the operating current of the motor flows through the motor windings. A metallic short circuit was modelled as shown in Fig. 1(b), thus the stator fault resistance of the damaged part of the motor tends to zero, i.e. $R_f \rightarrow 0$. A short-circuit loop is created in the faulty part through which the reverse short-circuit current flows ($-I_f$ in Eq. (2)). A similar approach to modelling short-circuit faults is presented in [30].

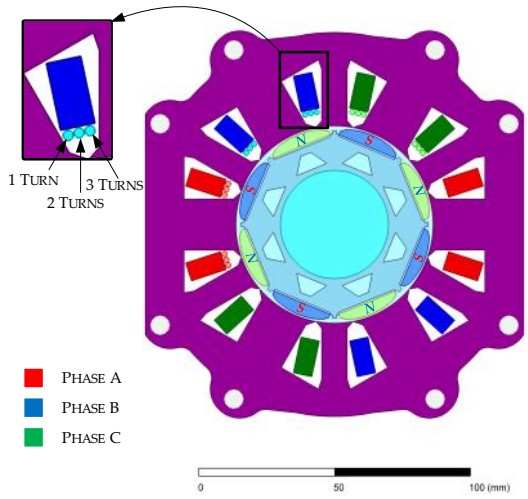

Fig. 2. FEM model of the PMSM with separate coils for modelling the interturn short-circuits

The process of the co-simulation of the field-circuit model is similar to the system presented in [22]. The data processing algorithm, presented in Fig. 3, can be divided into three stages: initialisation, calculations, and data recording. The "*Initialisation*" step provides the information necessary for the correct configuration of *Ansys* and *MathWorks* software, i.e. selection of the calculation step, integration method, drive operating conditions, type of faults and setting parameters of the PI controllers of the FOC structure. Once correctly configured, the second main step, called the "*Co-simulation calculations of the PMSM*" process between *Simulink* and *Ansys Maxwell* follows. The *Twin Builder* environment is used to exchange the data correctly between the above-mentioned programs. Once in operation, the *Simulink* master software prepares all the

www.czasopisma.pan.pl PAN POLSKA AKADEMIA NAUK www.journals.pan.pl

necessary data to run the field-circuit model. The data includes signals such as phase voltages (calculated by the control structure), the type and severity of the failure and the value of the load torque. The collected dataset is passed to the motor model mentioned above, created with *Ansys Maxwell* software, where the actual values of the electromagnetic and mechanical variables of the overall motor model are calculated. As an effect, data on phase currents, speed and rotor position is transferred to *Simulink*, where the calculations for the next iteration are made. Once the simulation is finished, "*recorded data*" is written to a measurement file that contains the data that is used for the further analyses.

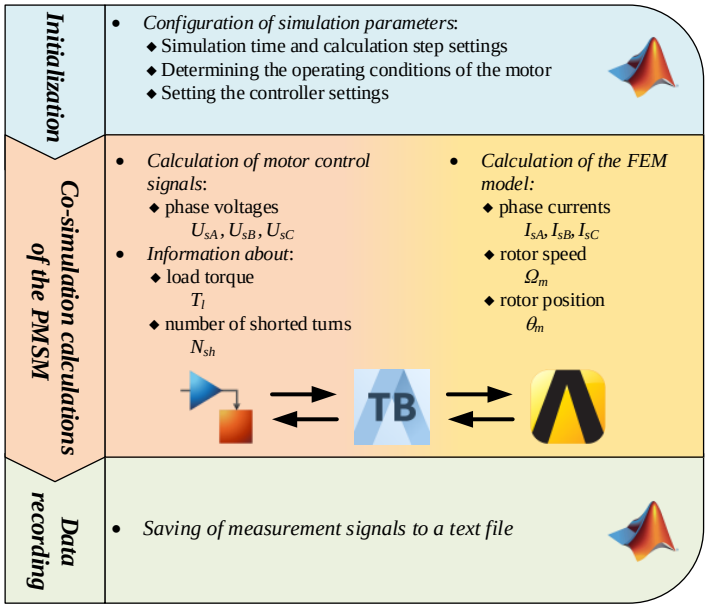

Fig. 3. Data processing procedure in co-simulation

3. Experimental test setup

The experimental setup is shown in Fig. 4. The tested 2.5 kW PMSM is a specially prepared motor, that allows for the manual modelling of multiple short circuits in each phase of the stator winding. During the tests the short-circuit fault was made using a connector with a negligible resistance, i.e. $R_f \rightarrow 0$. The PMSM under the tests is connected with another 4.7 kW PMSM that ensures the load torque.

The tested motor is powered with a voltage source inverter (VSI) by TWERD. A hardware dead-time is ensured by a specially prepared card that transforms electrical into fibre-optics signals. The braking resistor is controlled in a similar way. The control system is designed using MATLAB/Simulink software and operated in real-time with VeriStand by National Instruments

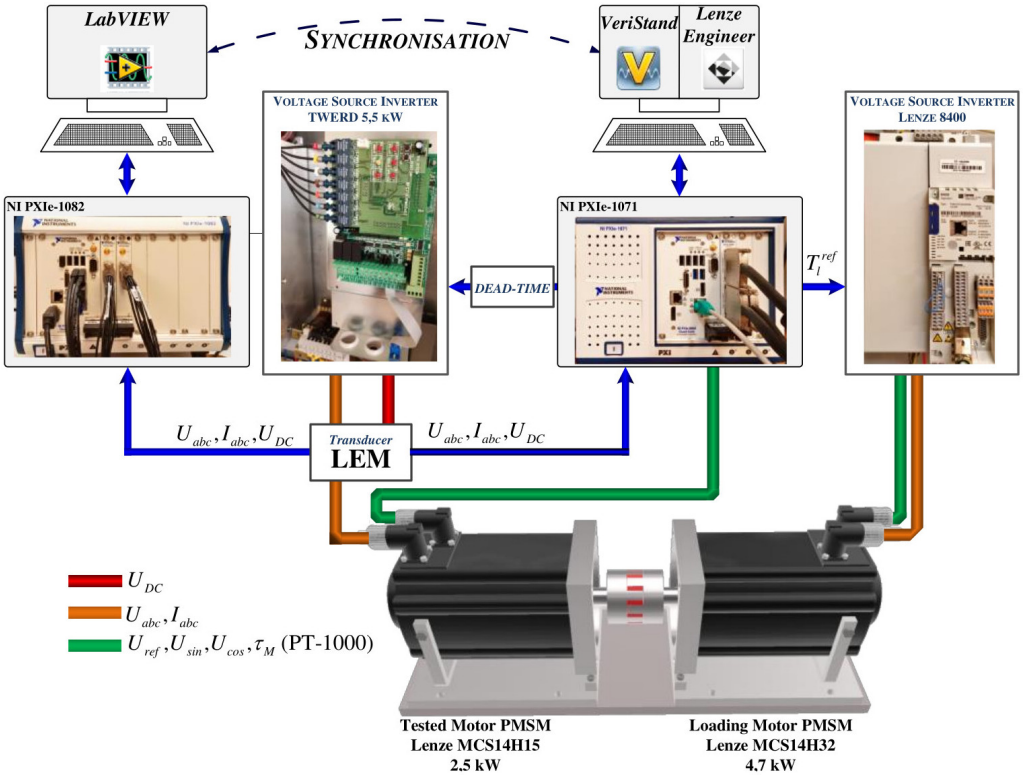

Fig. 4. Experimental test setup configuration

(NI). The computer with VeriStand software is connected to a NI PXI 1071 rapid prototyping system, equipped with an NI PXIe-8840 Quad-Core controller and an FPGA NI PXI-7852R card. The control loop was controlled at a 10 kHz frequency during all the tests.

The load motor is supplied with a Lenze TopLine C 8 400 frequency converter and programmed by Lenze Engineer software. The requested load torque value T_l^{ref} is transferred to the converter in an analogue way from NI PXI.

Second NI PXIe-1082 is equipped with two NI PXIe-4492 DAQ measurement cards. The PXI is connected to another PC with LabVIEW software. The DC-bus voltage U_{DC}, stator currents I_{abc} and voltages U_{abc} are measured by LEM transducers and then transferred to both PXIs. The signals are used to control the tested motor (PXIe-1071) and to diagnose its condition (PXIe-1082). The measured signals and the signals from the control structure, such as the stator current vector components I_{sd}, I_{sq}, stator voltage vector components U_{sd}, U_{sq}, as well as the decoupling signals E_{sd}, E_{sq} used in further analysis were sampled at a frequency equal to 8 192 (2^{13}) Hz.

Both motors are equipped with resolvers, therefore the reference U_{ref} and output modulated resolver signals $U_{\text{sin}}, U_{\text{cos}}$ are sent to the PXI and Lenze 8 400, respectively. The motor temperature τ_M is also measured by a PT-1 000 sensor and verified by control units.

www.czasopisma.pan.pl PAN POLSKA AKADEMIA NAUK www.journals.pan.pl

4. PMSM control structure

The upper part of Fig. 5 shows the applied control structure. For all analysed cases: the analytical model, the FEM-based model and the real object, as well as the control structure were identical and implemented in Simulink. The analytical model was implemented in Simulink as well (Fig. 5, bottom part, left), while the FEM model, as mentioned above, was created in Ansys Maxwell software (Fig. 5, bottom part, centre). The real motor is shown as a 3D object (Fig. 5, bottom part, right).

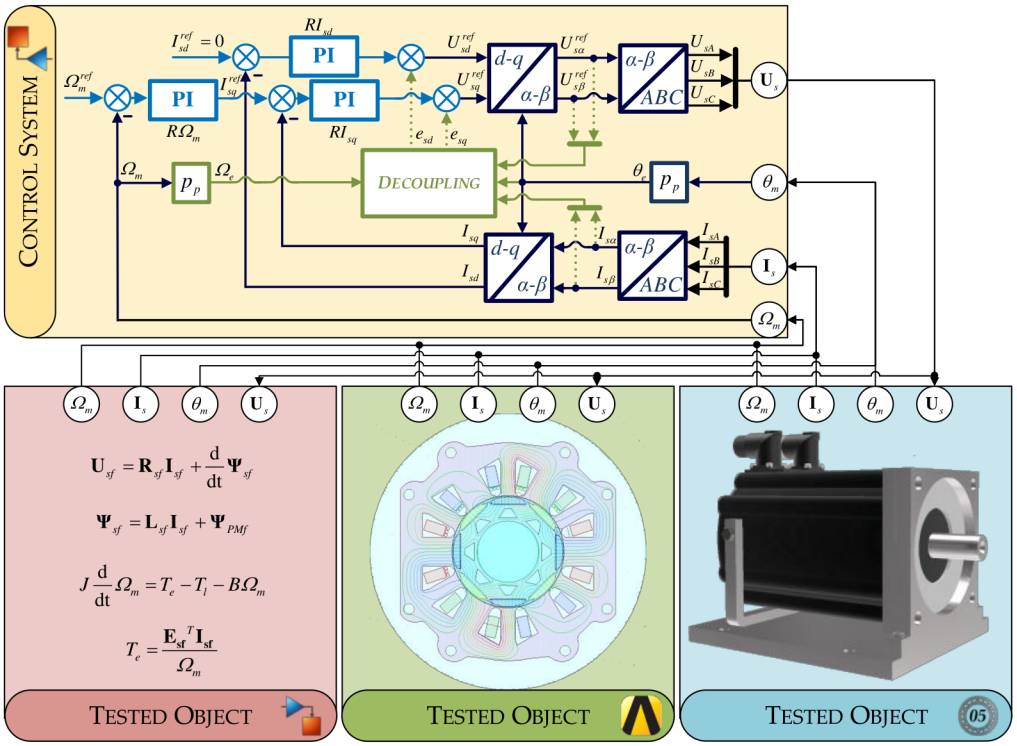

Fig. 5. Generalized block diagram of FOC structure co-operating with all three types of model used during the tests: the analytical model, the field-circuit model and real object

The control system is a classic field-oriented control (FOC) structure with three PI controllers that ensures a constant power angle (the angle between stator current and rotor flux vectors), equal to 90 degrees. Therefore, the reference d-axis stator current component is equal to zero, i.e. $I_{sd}^{\mathrm{ref}} = 0$. The reference q-axis current component is defined by the speed PI regulator, since the component is responsible for motor torque generation [31]. Assuming that the motor is undamaged:

$$T_e = \frac{3}{2} p_p \Psi_{PM} I_{sq} \,. \tag{11}$$

www.czasopisma.pan.pl PAN POLSKA AKADEMIA NAUK www.journals.pan.pl

The inner PI controllers are used in order to ensure that the reference and real values of stator current components follow each other. The outputs of the controllers are decoupled, using the decoupling signals E_{sd} and E_{sq}, calculated on the basis of electrical angle, speed and estimated stator flux components (with usage of measured currents and reference voltages). They can be calculated as follows [31]:

$$E_{sd} = -p_p \Omega_m \widehat{\Psi}_{sq} \,, \tag{12}$$

$$E_{sq} = p_p \Omega_m \widehat{\Psi}_{sd} \,. \tag{13}$$

The vector of the stator flux is estimated by (14). The applied estimator is based on the simplest estimation method that relies on the stator winding voltage balance equations expressed in a stationary frame, assuming a non-fault operation. Additionally, the simplest low-pass filter is applied (with a time constant T_f), which eliminates the problems with initial condition determination and the DC drift caused by the measurement sensor offsets [32].

The voltage vector components, necessary to determine the stator flux are estimated using the DC voltage, supplying the inverter and three inverter control signals:

$$\frac{\mathrm{d}\widehat{\boldsymbol{\Psi}}_{\boldsymbol{s}}}{\mathrm{d}t} = \boldsymbol{U}_s - R_s \boldsymbol{I}_s - \frac{1}{T_f}\hat{\boldsymbol{\Psi}}_{\boldsymbol{s}} \,. \tag{14}$$

All six components from the control structure, i.e. two current, two voltage and two decoupling vector components can possibly be used as diagnostic signals. The *d-q* reference voltages are transferred into ABC values using Clarke/Park inverse transformations and then they become the inputs of the simulation models, as shown in the bottom row of Fig. 5. Only in the case of the real motor, the Voltage Source Inverter with Space Vector Modulation (SVM) is used.

5. Diagnostic procedure

The process of inferring the current state of a PMSM is presented in Fig. 6. It is necessary to know the characteristics of the tested object and to select some potential signals, which may carry the information about possible damage. The following steps can be taken in order to diagnose the short-circuit fault:

- First of all, necessary physical signals are measured by their sensors. These are: phase currents, DC voltage and rotor position/speed. These signals are required by the control structure and they become the inputs of the FOC of PMSMs.
- The diagnostic signals must be selected in the second step. In this paper the possibility to use six mentioned signals from the control structure: *d-q* axis current, voltage and decoupling signal components is evaluated. All the signals will be verified in further sections.
- Thus, the selected signals are acquired from the control structure and based on the classic methods of signal analysis (such as the FFT), the signal spectra are calculated. By analysing the obtained spectra, the damage symptoms are extracted, and on the basis of information about changes in their amplitude, it is possible to estimate whether the tested motor is damaged or not. Searching for the symptoms is the most important part of the research presented in this study.

– Finally, some decision system must be applied, that can infer about the condition of the machine. In this paper a simple threshold-level based system is presented. In this system, the amplitude of the fault frequency is compared with its value for a healthy machine in different operating states of the drive. If the *warning threshold* is exceeded the *warning* state is indicated, while the *fault threshold* is exceeded the *defect* is found and the drive should be stopped. Thus, the degree of the damage is assessed in order to plan the maintenance of the machine.

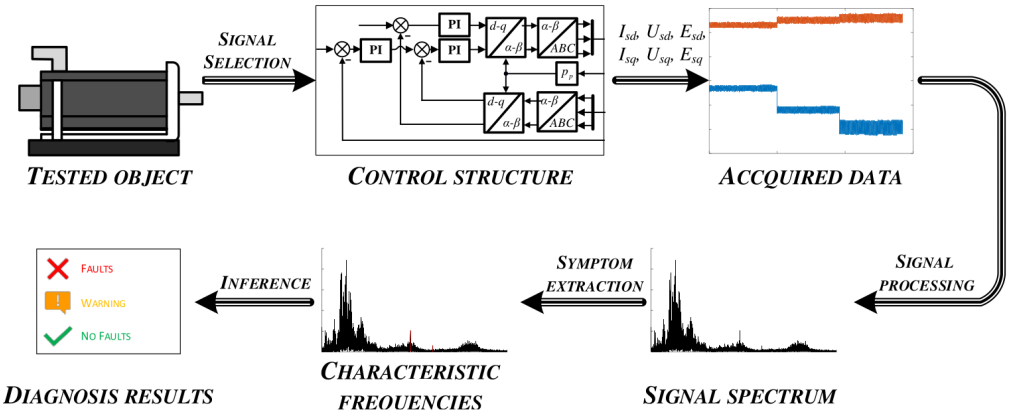

Fig. 6. The diagnostic process based on signals from the control structure

The stator fault analysis will be carried out for the Lenze 14H15 synchronous motor. The parameters used in both simulation models are summarised in Table 2 in Appendix. As will be shown in further section, the effective fault indicator can be selected as twice the fundamental supply frequency.

6. Obtained results

6.1. Verification of the analyzed PMSM mathematical models

In order to extract the stator winding fault symptoms, a series of simulations of analytical and the field-circuit models were performed for different operating conditions of the drive in the range of $f_s = 10-100$ Hz under load conditions in the range of $T_l = 0-100\%$, together with the modelled initial motor fault in the range of $N_{sh} = 1-3$ shorted turns. An example of the mapping of selected signals for the PMSM drive at rated operating conditions and with the fault occurring in the form of three short-circuited turns is presented in Fig. 7.

The simulation models correctly reproduced the phenomena occurring in the physical object, which results from the comparison of the simulation results obtained with the experimental tests. In the case of rated operation, the mapping error of phase current amplitudes in a PMSM is below 5%, regardless of the analysed load or frequency.

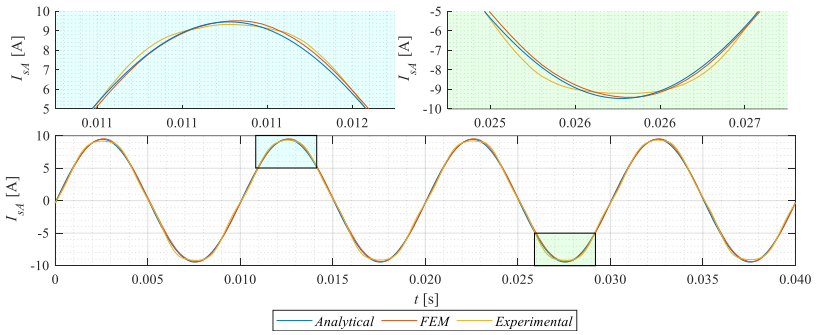

Fig. 7. Phase current transient during the fault in phase B, for different simulation models (analitycal, FEM) and experimental tests; $f_s = 100$ Hz, $T_l = T_N$, $N_{sh} = 3$

6.2. Analytical, FEM and experimental results comparison

In order to further verify the fundamental models presented in previous sections, the detailed comparative studies have been conducted. Figure 8 shows one of the control structure signals, i.e. the d-axis component of the stator current vector, which has been selected to further analysis. The analytical, FEM and experimental spectra are presented together to evaluate the similarities and differences for a different number of shorted turns ($N_{sh} = 0, 1, 2, 3$). The biggest and understandable difference is the base level of the presented spectra (Fig. 8(a)). It can be seen that the lowest level of noise is present in the case of the analytical model. As the component I_{sd} is defined in a rotating coordinate frame and is controlled to stay zero, there is no fundamental component of the signal. There are, however, some characteristic frequencies, mentioned above – twice the fundamental frequency, $2f_s$, (in this case it is equal to 200 Hz, as the supply frequency is 100 Hz) and four times the fundamental frequency, $4f_s$.

The amplitudes of the frequency $2f_s$ are increasing with the increasing number of shorted turns as shown in detail in Figs. 8(b)–8(d), for the experimental test, FEM and analytical models, respectively. It can be seen that the amplitude can be used as an efficient diagnostic index to distinguish between a healthy and faulty state of the machine. It can be seen that in the case of the experimental results and the FEM model, the increase of the amplitudes is relatively very similar. On the contrary, the analytical model presents a significant change between the 0 and 1 shorted turns, while for a bigger number of N_{sh}, the sensitivity to the increasing severity of the fault is much lower (Fig. 8(d)).

According to the above analysis, both the FEM and experimental results will be taken for further analysis in this paper, as the results obtained for the analytical model are greatly diverging. The detailed analysis of the control structure signals is shown in Figs. 9, 10 and 11. First, a series of FEM simulations have been conducted and the q-axis voltage, current and d-axis decupling voltage components are presented in Fig. 9. The d-axis component is presented here on purpose – it is calculated based only on q-axis variables (see Eq. (12)). All of the results shown below are obtained for 60% of the nominal frequency and 60% of nominal torque. However, the results for different frequencies and load torques have been also analysed, and the qualitative results are

www.czasopisma.pan.pl PAN POLSKA AKADEMIA NAUK www.journals.pan.pl

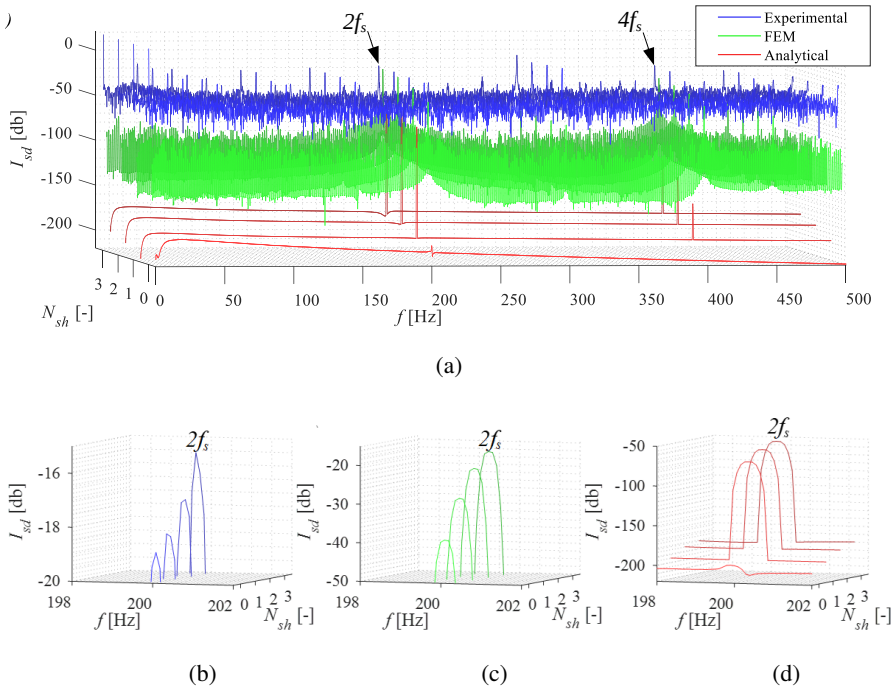

Fig. 8. Comparison of different models spectra for control structure signal I_{sd} during the fault in phase B, for supply frequency $f_s = 100$ Hz and different numbers of shorted turns N_{sh}: (a) summary of the spectra analysed; (b), (c), (d) zoom of the $2f_s$ component

analogical. The upper row of the figures shows the dependence of the fault indicator on the supply frequency, while the bottom row shows its relation to the load torque level.

The frequency has a much greater impact on the level of twice the fundamental frequency, compared to the load torque. As can be seen, value of the fault indicator increases greatly with the frequency level, especially when the frequency is lower than around 80 Hz. However, for each frequency value, the fault indicator increases and the level of the increase is higher with higher frequencies. The behaviour of the decoupling voltage component, E_{sd}, is very similar to the voltage component, U_{sq}. However, its sensitivity is slightly higher for very low frequencies. On the other hand, the amplitudes of the $2f_s$ frequency in the stator current component, I_{sq}, are quite puzzling and generally decrease between supply frequencies 10 Hz and 60 Hz and then increase again up to the nominal speed. The reason of this is unknown – it will be a further step in future research. Probably, it can be connected with a specific structure of the motor under the test. Nevertheless, it makes the q-axis current a poor diagnostic signal.

The influence of the load torque (bottom row of Fig. 9) is much lower. Especially, the voltage and decoupling-based signals are almost independent on the disturbance level.

In order to verify the FEM modelling-based simulations, extended experimental tests have been conducted (Fig. 10). Two main features of the components are similar. They increase significantly with the frequency and do not depend on the load torque. However, there are a lot of

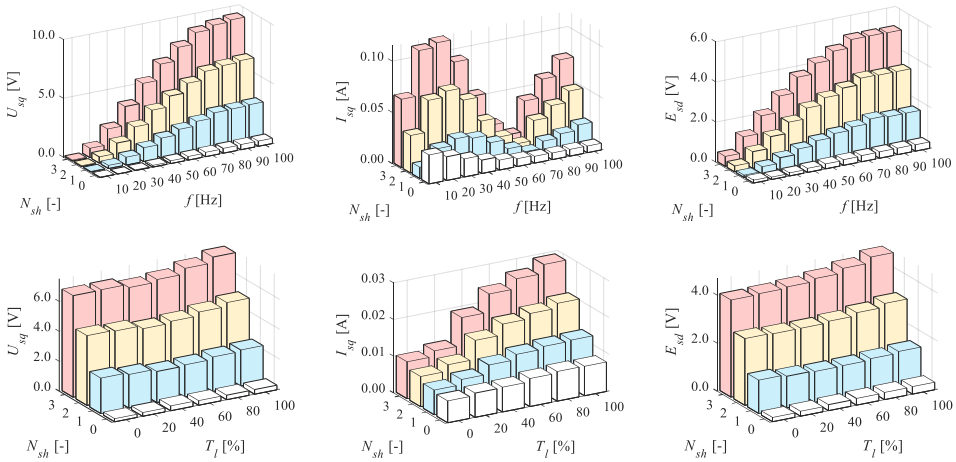

Fig. 9. Fault indices based on: q-axis voltage (left), q-axis current (center), d-axis decoupling voltage (right) as a function of the number of shorted turns. Dependence on supply frequency (first row, load torque 60% T_N) and load torque (second row, supply frequency 60 Hz); FEM modelling

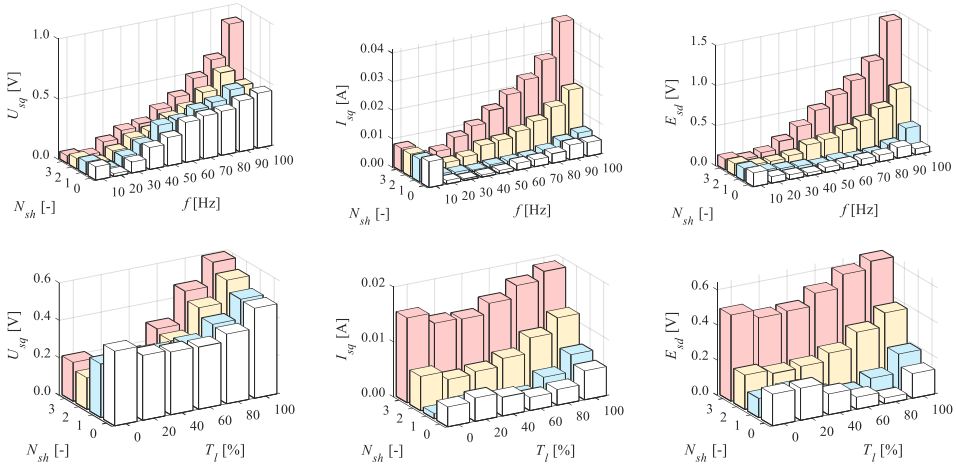

Fig. 10. Fault indices based on: q-axis voltage (left), q-axis current (center), d-axis decoupling voltage (right) as a function of the number of shorted turns. Dependence on supply frequency (first row, load torque 60% T_N) and load torque (second row, supply frequency 60 Hz); experimental tests

negative phenomena that reduce possible applicability of the q-axis-based signals in the diagnosis of interturn short circuits. First, there are frequencies where the level of the fault indicator is larger for no faulty operation compared to the damaged operation ($N_{sh} > 0$). It is especially visible in Fig. 10 (bottom, left), in the case of the q-axis voltage component. However, the behaviour of the decoupling signals is much more correct and the diagnosis for the number of shorted turns

www.czasopisma.pan.pl PAN POLSKA AKADEMIA NAUK www.journals.pan.pl

$N_{sh} > 1$ should be effective. Concluding, based on the FEM simulation and experimental results, the q-axis signals should be treated as ineffective diagnostic signals.

Unlike the quadrature axis signals, Fig. 11 shows the characteristics of the direct axis components. It is shown that all voltage, current and decoupling components can be successfully applied in the diagnosis of the interturn short circuits. As it was shown previously, the amplitudes of the proposed fault indicators increase with the supply frequency and stay almost constant with varying load torque. The decision about the fault can be made comparing the healthy and actual level of the selected components. However, a simple classic neural network can be applied to automate the diagnostic process. All three d-axis components and the supply frequency can be selected as the inputs of the network. This will be further analysed in the future.

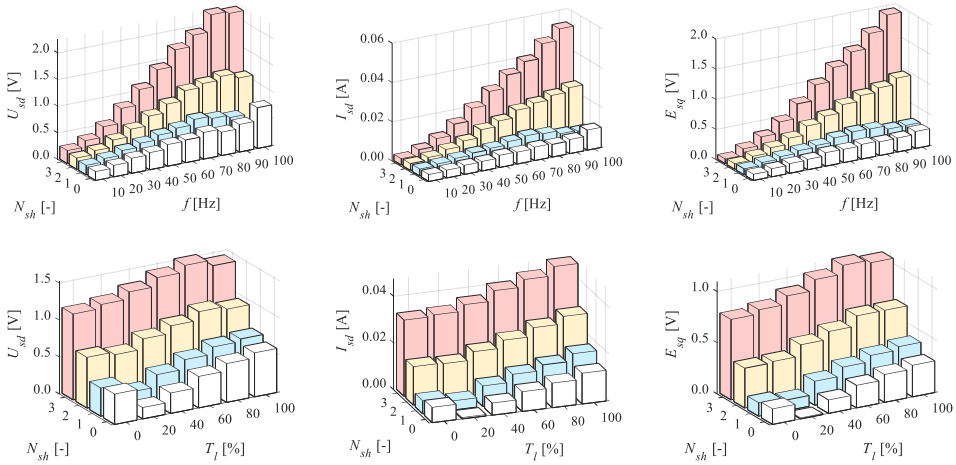

Fig. 11. Fault indices based on: d-axis voltage (left), d-axis current (center), q-axis decoupling voltage (right) as a function of the number of shorted turns. Dependence on supply frequency (first row, load torque 60% T_N) and load torque (second row, supply frequency 60 Hz); experimental tests

6.3. Online operation of the diagnostic process

The online operation of the diagnostic process is shown in Fig. 12 and Fig. 13. Due to the limited number of pages, only the diagnostic inference based on the reference d-axis component of the voltage vector is presented. Both figures present the operation with constant speed of the drive, while the load torque is changing from zero, through 40% up to 80% of the nominal value (to clarify the figures, the dynamical processes have been removed). In both cases the motor starts its operation as a healthy device and later, for each value of the load torque, different levels of the interturn short-circuit fault were modelled for several seconds – the number of shorted turns is equal to $N_{sh} = 1$, $N_{sh} = 2$ and finally $N_{sh} = 3$, respectively.

As it can be seen in Fig. 12, the oscillation level of the analysed component is increasing when the fault occurs. However, the oscillation level cannot be selected directly as the fault indicator, as it is changing with the operation point, including changing load torque and speed levels. Similarly, the mean value of the component is useless in this purpose, as it is significantly varying with

www.czasopisma.pan.pl PAN POLSKA AKADEMIA NAUK www.journals.pan.pl

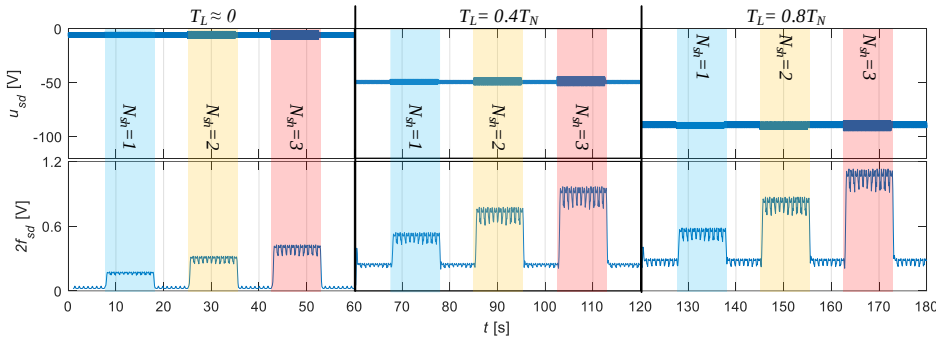

Fig. 12. Online operation of the diagnostic process: instantaneous value (upper) of the d-axis voltage vector component and the fault index and its second harmonic (lower) for constant, nominal speed and different values of the load torque; FEM simulation results

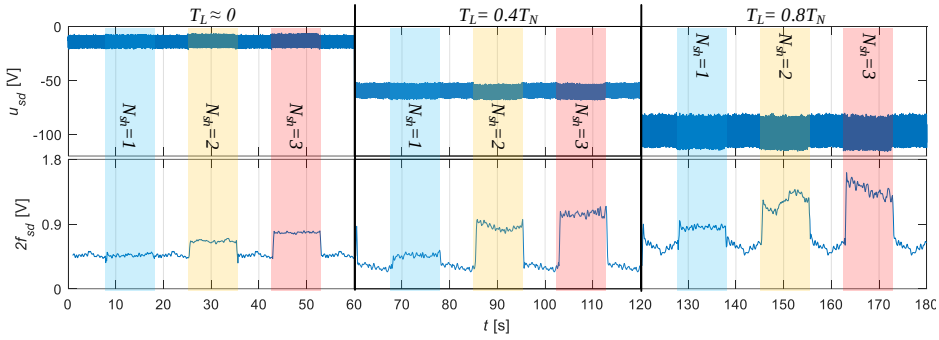

Fig. 13. Online operation of the diagnostic process: instantaneous value (upper) of the d-axis voltage vector component and the fault index and its second harmonic (lower) for constant, nominal speed and different values of the load torque; experimental results

load torque value. The value of the $2f_s$ amplitude of the analysed U_{sd} component is shown in the bottom part of the figure. The mentioned amplitude increases considerably when the short-circuit fault appears ($N_{sh} > 0$). It can be seen as the step-wise waveforms that return to a healthy value after the fault disappears. This healthy-value level is much lower during the idle operation than during the load operation. However, the no load operation is not possible in a real drive.

As it is shown in both figures, the level of the diagnostic signal is greatly higher when the fault occurs than in the case of the non-fault operation. Even one shorted turn can be detected by taking FEM modelling into account. However, detecting one shorted turn in the case of real motor operation can be problematic, especially when the load torque is low or close to zero. It is shown in the bottom part of Fig. 13. However, when the number of shorted turns is higher ($N_{sh} > 2$), the difference between non-faulty and faulty operation allows one to successfully detect the analysed fault.

www.czasopisma.pan.pl PAN POLSKA AKADEMIA NAUK www.journals.pan.pl

6.4. Evaluation of all control structure virtual signals

Based on the results presented in this paper and a detailed analysis, not presented here due to the limited number of pages, the summary of the control structure-based signals is presented in Table 1. The table is divided into two main parts: operation with and without the control path decoupling. All six signals from the control structure are compared. It can be seen that if only the analytical model is applied all of the analysed signals can be successfully used as the diagnostic signals. However, when the detailed analysis is conducted using FEM modelling, usefulness of the q-axis-based signals (especially q-axis current component) in the interturn short-circuit diagnosis decreases. This relationship is further deepened in the experimental validation. The same is true for the q-axis voltage component and d-axis decoupling signal component (as it depends on q-axis signals).

Table 1. Comparison/evaluation of all diagnostic signals

Signals	Without decoupling			Decoupling		
	Analytical	FEM	Experimental	Analytical	FEM	Experimental
I_{sd}	✓	✓	✓	✓	✓	✓
I_{sq}	✓	X/✓	X	✓	X/✓	X
U_{sd}	✓	✓	✓	✓	✓	✓
U_{sq}	✓	✓	X	✓	✓	X
E_{sd}	–	–	–	✓	✓	X/✓
E_{sq}	–	–	–	✓	✓	✓

The conclusions for the case without and with the decoupling of the control paths are quite similar. However, the number of available diagnostic signals is lower when the decoupling is not applied.

Other faults or anomalies can affect the occurrence of additional harmonics as shown in [33]. The authors considered the eccentricity of the machine and the effect of rotor design on motor operation. The stator radial tooth force spectrum is presented for a motor with 6 pairs of poles in Fig. 6 and Fig. 7 (in [33]). The study shows that for $3f_s = 18f_r$ (f_r is the rotational frequency), the amplitude in the spectrum takes insignificant values, which allows one to conclude that it slightly affects the analysed symptoms of short-circuit damage. After the analysis, it was noted that this symptom transfers to the d-q axis based control system in the form of $2f_s$ frequency.

On the other hand, in [34], the authors analysed the impact of different current sensor faults, as can be seen in Fig. 4 (in [34]), where the current and speed waveforms of the open circuit are presented. After the disappearance of the measured signal in phase A, a signal with a frequency of $2f_s$ appears in the d-q axis signals, however, its amplitude is about 33.3% of the value of the amplitude of the supply signal, which would rapidly affect the results obtained, in addition, it would disturb the operation of the entire control system.

A comparison between the short-circuit fault and demagnetization fault is presented in [35]. As can be seen in Fig. 8 (in [35]), the effect of the appearance of damage symptoms for a $2f_s$ short circuit is evident, but it is independent on the occurrence of the demagnetization.

www.czasopisma.pan.pl PAN POLSKA AKADEMIA NAUK www.journals.pan.pl

7. Conclusions

The paper presents the possibility to diagnose interturn short-circuits fault occurring inside PMSM stator windings using the signals from the control structure. Six signals are taken into consideration: two components of stator voltage, current and decoupling signal vectors. The main emphasis is put on modelling the fault in different ways: analytical, FEM-based and real, experimental motor models. It is shown that the analytical model can be only used to design and initially verify the diagnostic methods, as the results are obtained almost immediately due to very short simulation time, comparing to remaining methods. As it is presented here, the designed diagnostic algorithms should be then further evaluated, at least using detailed FEM modelling with detailed designed motor parameters, especially when the real machine to be diagnosed cannot be physically modified.

The proposed diagnostic method is based on the virtual control structure signals. It is shown that the fault indicators based on those signals can be successfully used in the diagnostic as their values increase with the increasing level of the damage. Moreover, they are almost independent of the load torque value. However, the diagnostic system has to be based also on the supply frequency, as the values of the fault indices grow with the increasing speed of the motor. Thus, the diagnostic system must be based on different threshold levels, dependent on the supply frequency or a simple neural network must be applied, while its inputs can be selected components from the control structure and the supplying frequency value.

After careful analysis, the components based on the direct axis variables are proved to be the most effective diagnostic signals. They are d-axis voltage, d-axis current and q-axis decoupling signals, as it is calculated using the first two variables and speed. The amplitudes of second order harmonics of the mentioned signals are proposed to be the fault indicators.

The presented diagnostic algorithm is based on the signals that are available in the control structure, therefore no additional sensor is required. It is only necessary to calculate the FFT algorithm to determine the amplitude of the second order harmonics. However, in the case of applied modern microprocessor-based systems this is not a problem.

Future research includes the application of a classical neural network based on the control structure signals and evaluation of its efficiency. Moreover, the influence of the PI controller parameters on the overall diagnostic method will be verified.

Appendix

The parameters and nominal data of the motor under test are shown in Table 2.

Table 2. Parameters and nominal data of tested PMSM

Parameter name	Symbol	Value	Unit
Power	P_N	2 500	W
Torque	T_N	16	Nm
Speed	n_N	1 500	r/min
Stator phase voltage	U_{sN}	325	V

www.czasopisma.pan.pl PAN POLSKA AKADEMIA NAUK www.journals.pan.pl

Table 2 [cont.]

Parameter name	Symbol	Value	Unit
Stator current	I_{sN}	6.6	A
Frequency	f_{sN}	100	Hz
Pole pairs number	p_p	4	–
Number of stator winding turns	N_s	2×125	–
Moment of inertia	J	1.42	kg·cm^2
Remanent magnetization	B_r	1.27	T
Stator resistance	R_s	1.206	Ω
Stator inductance	L_s	20.62	mH

Acknowledgements

This work was supported by the National Science Centre Poland under grant 2017/27/B/ST7/00816.

References

[1] Mishra A., Agarwal P., Srivastava S.P., *A comprehensive analysis and implementation of vector control of permanent magnet synchronous motor*, International Journal of Power and Energy Conversion, vol. 5, no. 1, pp. 1–23 (2014), DOI: 10.1504/IJPEC.2014.059982.

[2] Chen Y., Liang S., Li W., Liang H., Wang C., *Faults and Diagnosis Methods of Permanent Magnet Synchronous Motors: A Review*, Applied Sciences, vol. 9, no. 10, pp. 2116–2132 (2019), DOI: 10.3390/app9102116.

[3] Orlowska-Kowalska T., Wolkiewicz M., Pietrzak P., Skowron M., Ewert P., Tarchala G., Krzysztofiak M., Kowalski C.T., *Fault Diagnosis and Fault-Tolerant Control of PMSM Drives–State of the Art and Future Challenges*, IEEE Access, vol. 10, pp. 59979–60024 (2022), DOI: 10.1109/ACCESS.2022.3180153.

[4] Cardoso A.J.M., *Diagnosis and Fault Tolerance of Electrical Machines, Power Electronics and Drives*, IET – The Institution of Engineering and Technology (2018).

[5] Ge Y., Song B., Pei Y., Mollet Y.A.B., Gyselinck J.J.C., *Analytical Expressions of Isolation Indicators for Permanent-Magnet Synchronous Machines Under Stator Short-Circuit Faults*, IEEE Transactions on Energy Conversion, vol. 34, no. 2, pp. 984–992 (2019), DOI: 10.1109/TEC.2018.2878343.

[6] Gao F., Zhang G., Li M., Gao Y., Zhuang S., *Inter-turn fault identification of surface-mounted permanent magnet synchronous motor based on inverter harmonics*, Energies, vol. 13, no. 4, pp. 899–912 (2020), DOI: 10.3390/en13040899.

[7] Romeral L., Urresty J.C., Riba Ruiz J.-R., Garcia Espinosa A., *Modeling of Surface-Mounted Permanent Magnet Synchronous Motors with Stator Winding Interturn Faults*, IEEE Transactions on Industrial Electronics, vol. 58, no. 5, pp. 1576–1585 (2011), DOI: 10.1109/TIE.2010.2062480.

[8] Farooq J.A., Raminosoa T., Djerdir A., Miraoui A., *Modelling and simulation of stator winding inter-turn faults in permanent magnet synchronous motors*, COMPEL-The International Journal for Computation and Mathematics in Electrical and Electronic Engineering, vol. 27, no. 4, pp. 887–896 (2008), DOI: 10.1108/03321640810878306.

www.czasopisma.pan.pl PAN POLSKA AKADEMIA NAUK www.journals.pan.pl

[9] Boileau T., Leboeuf N., Nahid-Mobarakeh B., Meibody-Tabar F., *Synchronous demodulation of control voltages for stator interturn fault detection in PMSM*, IEEE Transactions on Power Electronincs, vol. 28, no. 12, pp. 5647–5654 (2013), DOI: 10.1109/TPEL.2013.2254132.

[10] Meinguet F., Semail E., Kestelyn X., Mollet Y., Gyselinck J., *Change-detection algorithm for short-circuit fault detection in closed-loop AC drives*, IET Electric Power Applications, vol. 8, no. 5, pp. 165–177 (2014), DOI: 10.1049/iet-epa.2012.0316.

[11] Mazzoletti M.A., Bossio G.R., De Angelo C.H., Espinoza-Trejo D.R., *A Model-Based Strategy for Interturn Short-Circuit Fault Diagnosis in PMSM*, IEEE Transactions on Industrial Electronics, vol. 64, no. 9, pp. 7218–7228 (2017), DOI: 10.1109/TIE.2017.2688973.

[12] Hang J., Zhang J., Xia M., Ding S., Hua W., *Interturn Fault Diagnosis for Model-Predictive-Controlled-PMSM Based on Cost Function and Wavelet Transform*, IEEE Transactions on Power Electronics, vol. 35, no. 6, pp. 6405–6418 (2020), DOI: 10.1109/TPEL.2019.2953269.

[13] Wu C., Jiang S., Bian C., *Online parameter identification of SPMSM based on improved artificial bee colony algorithm*, Archives of Electrical Engineering, vol. 70, no. 4, pp. 777–790 (2021), DOI: 10.24425/aee.2021.138260.

[14] Hang J., Zhang J., Ding S., Huang Y., Wang Q., *A Model-Based Strategy with Robust Parameter Mismatch for Online HRC Diagnosis and Location in PMSM Drive System*, IEEE Transactions on Power Electronics, vol. 35, no. 10, pp. 10917–10929 (2020), DOI: 10.1109/TPEL.2020.2978139.

[15] Fonseca D.S.B., Santos C.M.C., Cardoso A.J.M., *Stator Faults Modeling and Diagnostics of Line-Start Permanent Magnet Synchronous Motors*, IEEE Transactions on Industry Applications, vol. 56, no. 3, pp. 2590–2599 (2020), DOI: 10.1109/TIA.2020.2979674.

[16] Yang Z., Chen Y., *Interturn Short-Circuit Fault Detection of a Five-Phase Permanent Magnet Synchronous Motor*, Energies, vol. 14, no. 2, pp. 434–451 (2021), DOI: 10.3390/en14020434.

[17] Jeong H., Lee H., Kim S.W., *Classification and Detection of Demagnetization and Inter-Turn Short Circuit Faults in IPMSMs by Using Convolutional Neural Networks*, IEEE Energy Conversion Congress and Exposition (ECCE), Portland, USA, pp. 3249–3254 (2018), DOI: 10.1109/ECCE.2018.8558191.

[18] Huang S., Aggarwal A., Strangas E.G., Li K., Niu F., Huang X., *Robust Stator Winding Fault Detection in PMSMs with Respect to Current Controller Bandwidth*, IEEE Transactions on Power Electronics, vol. 36, no. 5, pp. 5032–5042 (2020), DOI: 10.1109/TPEL.2020.3030036.

[19] Skowron M., Orlowska-Kowalska T., Kowalski C.T., *Detection of permanent magnet damage of PMSM drive based on direct analysis of the stator phase currents using convolutional neural network*, IEEE Transactions on Industrial Electronics, vol. 69, no. 12, pp. 13665–13675 (2022), DOI: 10.1109/TIE.2022.3146557.

[20] Moosavi S.S., Djerdir A., Ait-Amirat Y., Khaburi D.A., *ANN based fault diagnosis of permanent magnet synchronous motor under stator winding shorted turn*, Electric Power Systems Research, vol. 125, pp. 67–82 (2015), DOI: 10.1016/j.epsr.2015.03.024.

[21] Fitouri M., Bensalem Y., Abdelkrim M.N., *Modeling and detection of the short-circuit fault in PMSM using Finite Element Analysis*, IFAC-PapersOnLine, vol. 49, no. 12, pp. 1418–1423 (2016), DOI: 10.1016/j.ifacol.2016.07.769.

[22] Sun W., Hang J., Ding S., Hu Q., Ren X., *Electromagnetic Parameters Analysis of Inter-Turn Short Circuit Fault in DTP-PMSM Based On Finite Element Method*, 8th International Conference on Power Electronics Systems and Applications (PESA), Hong Kong, China, pp. 1–4 (2020), DOI: 10.1109/PESA50370.2020.9344033.

[23] Qiu H., Zhang Y., Yang C., Yi R., *Performance analysis and comparison of PMSM with concentrated winding and distributed winding*, Archives of Electrical Engineering, vol. 69, no. 2, pp. 303–317 (2020), DOI: 10.24425/aee.2020.133027.

www.czasopisma.pan.pl PAN POLSKA AKADEMIA NAUK www.journals.pan.pl

[24] Pietrzak P., Wolkiewicz M., *Comparison of Selected Methods for the Stator Winding Condition Monitoring of a PMSM Using the Stator Phase Currents*, Energies, vol. 14, no. 6, pp. 1630–1653 (2021), DOI: 10.3390/en14061630.

[25] Pietrzak P., Wolkiewicz M., *Stator winding fault detection of permanent magnet synchronous motors based on the bispectrum analysis*, Bulletin of the Polish Academy of Sciences: Technical Sciences, vol. 70, no. 2, pp. 1–11 (2022), DOI: 10.24425/bpasts.2022.140556.

[26] Pietrzak P., Wolkiewicz M., *On-line Detection and Classification of PMSM Stator Winding Faults Based on Stator Current Symmetrical Components Analysis and the KNN Algorithm*, Electronics, vol. 10, no. 15, p. 1786 (2021), DOI: 10.3390/electronics10151786.

[27] Wang B., Wang J., Griffo A., Sen B., *Stator turn fault detection by second harmonic in instantaneous power for a triple-redundant fault-tolerant PM drive*, IEEE Transactions on Industrial Electronics, vol. 65, no. 9, pp. 7279–7289 (2018), DOI: 10.1109/TIE.2018.2793188.

[28] Yao Y., Li Y., Yin Q., *A novel method based on self-sensing motor drive system for misalignment detection*, Mechanical Systems and Signal Processing, vol. 116, pp. 217–229 (2019), DOI: 10.1016/j.ymssp.2018.06.030.

[29] Phung V.T., Pacas M., *Sensorless harmonic speed control and detection of bearing faults in repetitive mechanical systems*, IEEE 3rd International Future Energy Electronics Conference and ECCE Asia (IFEEC 2017 – ECCE Asia), Kaohsiung, Taiwan, pp. 1646–1651 (2017), DOI: 10.1109/IFEEC.2017.7992294.

[30] Quintal-Palomo R., Dybkowski M., *Modelling and co-simulation of small wind turbine with permanent magnet synchronous generator*, Przegląd Elektrotechniczny, vol. 1, no. 10, pp. 210–215 (2019), DOI: 10.15199/48.2019.10.45.

[31] Mohamed Y.A.R.I., Radwan A.A.A., Lee T.K., *Decoupled reference-voltage-based active DC-link stabilization for PMSM drives with tight-speed regulation*, IEEE Transactions on Industrial Electronics, vol. 59, no. 12, pp. 4523–4536 (2011), DOI: 10.1109/TIE.2011.2182013.

[32] Zelechowski M., *Space Vector Modulated–Direct Torque Controlled (DTC–SVM) Inverter–Fed Induction Motor Drive*, Warsaw University of Technology, Ph.D. Thesis, Warsaw (2005).

[33] Jaeger M., Drichel P., Schröder M., Berroth J., Jacobs G., Hameyer K., *On magnetization deviations as the dominant cause for vibration harmonics in the spectrum of a PMSM drive*, Archives of Electrical Engineering, vol. 70, no. 3, pp. 719–730 (2021), DOI: 10.24425/aee.2021.137584.

[34] Jankowska K., Dybkowski M., *A current sensor fault tolerant control strategy for PMSM drive systems based on Cri markers*, Energies, vol. 14, no. 12, p. 3443 (2021), DOI: 10.3390/en14123443.

[35] Skowron M., Krzysztofiak M., Orłowska-Kowalska T., *Application of PMSM fault detector based on Kohonen classifier and FEM model*, International Symposium on Power Electronics, Electrical Drives, Automation and Motion (SPEEDAM), Sorrento, Italy, pp. 814–819 (2022), DOI: 10.1109/SPEEDAM53979.2022.9842181.